Foamability Properties of Low GWP Refrigerant and Oil Mixtures (ASHRAE RP-1879)

Kyle F.A. SHEPARD[1]*, Craig R. BRADSHAW[1]

[1]Center for Integrated Building Systems, Oklahoma State University
Stillwater, OK, USA
Phone – (580) 352-4395, Email – kyle.a.shepard@okstate.edu

* Corresponding Author

ABSTRACT

Oil-refrigerant mixture foaming is common in compressors found in many HVAC systems. Low-GWP refrigerants, particularly HFOs and blends, have under-studied foaming behavior and characterizing and understanding foaming behavior is necessary for the integration of new refrigerants in vapor compression cycles. In this work, an apparatus is designed and fabricated to study oil-refrigerant pairs in three manners: 1) physical foaming characterization, 2) measurement of dynamic surface tension between oil-refrigerant media, and 3) measurement of oil-refrigerant solubility data. Foaming is generated through pressure drop by charging and heating a chamber of refrigerant and oil and rapidly connecting it to a low-pressure chamber. Dynamic surface tension data is measured in post-processing via maximum bubble pressure tensiometry (MBPT). Foaming and dynamic surface tension experiments are visually recorded with a custom made, high-pressure sight glass which utilizes pressurized water to attain higher internal oil-refrigerant pressures. Physical characterization of foaming and bubbles is carried out in post-processing with camera-tracking software. Solubility is experimentally determined with a circulation loop containing a viscometer and a densitometer and thermodynamic correlations. The completed apparatus will be used to characterize the behavior of 11 pairs of refrigerant-lubricants including various viscosity grades of mineral oil, POE, PAG, and PVE lubricants paired with HFC and HFO refrigerants.

1. INTRODUCTION

Since the development of the Montreal Protocol and subsequent Kigali Amendment in 2016, there has been a large push for integrating low-GWP refrigerants into vapor compression cycle systems. Many of these new refrigerants require comprehensive, systematic studies to optimize design and performance characteristics within vapor compression cycles. Starting the compressor causes a foam column of refrigerant and oil to grow due to rapid depressurization evaporating refrigerant solved within and liquidated below the oil. Frequent and persistent foam columns cause oil migration into unwanted areas, becoming a performance and reliability concern for compressor manufacturers (Yangisawa *et al.* (1991), Fortkamp and Barbosa (2015)). Oil, an incompressible fluid, can cause damage to compression chambers due to excessively large hydraulic forces. An injection of excess oil into various components can also increase oil circulation rate, reducing system efficiency. Oil impacts heat transfer properties in nucleate boiling (Wang *et al.* (1999), Hung *et al.* (2016)), which is especially prominent in the evaporator. Foaming can also cause high-speed gearing, high-volume pumping, splash lubrication, cavitation, and overflow loss of refrigerant (ASTMD892 2003, ASTMD892 2018). Excessive and lingering oil-refrigerant foams can harm system performance and are a source of damage and inefficiency in compressors.

To mitigate issues caused by oil-refrigerant foams, it is necessary to study and understand them. This experimental study focuses on three properties of foams in a single experimental apparatus:

1) Qualitative and comparative foaming characterization.
2) Measurement of dynamic surface tension in oil-refrigerant media.
3) Measurement of solubility data.

Previous studies have been performed on oil-refrigerant foams. Yanagisawa *et al.* (1986) studied R22 and oil mixture foams from 20°C to 60°C below and exceeding saturation pressures, studying foaming generated by blade rotation

and direct vapor blowing. For several CFCs, HCFCs and HFCs and respective compatible oils between POE and mineral oils, Goswami *et al.* (1997) provided a comprehensive study studying viscosity, static and dynamic surface tension, foam growth and decay, absorption and desorption rates. Foam columns were experimentally created in two methods, one via ASTM-D892 with aeration of refrigerant into oil, and one via a pressure drop method. Pressure-drop induced foaming data by Goswami *et al.* (1997) was limited to total pressures around 1000 kPa, and only explored pressure drop ranges up to approximately 480 kPa. Largely, this study studied a wide range of refrigerant and oil pairs, however, new data is needed for newer refrigerant and oil pairs. The pressure drop method closely simulates the mechanisms by which foam is generated in vapor compression cycle compressors, though ignores mechanical stirring as used in Yanagisawa *et al.* (1991). Fortkamp and Barbosa Jr. (2016) provided a recent study on the foaming of R-134a and R-1234yf with POE oil mixtures, studying generated foam via pressure drop method and measuring foam height over time. To best emulate real oil-refrigerant foaming conditions in compressors, the experimental apparatus is designed to create pressure-drop induced foam.

Surface tension of refrigerants and oils has been studied in a variety of methods, however the maximum bubble pressure tensiometry method (MBPT) remains useful due to its accuracy for short bubble adsorption times (Liggieri, Mileva, Miller (2019)). MBPT is well-described in Fainerman and Miller (2004). Goswami *et al.* (1997) measured the static and dynamic surface tension of various CFC, HCFC, and HFC refrigerants with compatible POE and mineral oils via both Wilhelmy plate and MBPT methods. It should be noted that surface tension studies were performed only at atmospheric pressures. Seeton and Hrnjak (2009) studied the surface tension of CO2 and POE oil via MBPT. Fukuta *et al.* (2017) studied the surface tension of CO2 and PAG mixtures via MBPT. With similar models to Fukuta *et al.* (2017), Lee *et al.* (2022) used MBPT methods to study R410a and PVE oil. The maximum bubble pressure tensiometry method remains an accurate and widely used method for determining the surface tension of two-component systems.

Common solubility studies for two-component mixtures in the HVAC&R industry often measure the viscosity, density, temperature, and pressure and correlate these measurements to mass fractions (solubility) in multi-component thermodynamic models. Yokozeki (1994) utilized two fitted models: a modified Wilson activity coefficient model and a Soave-Redlich-Kwong equation of state combined with a mixing model. To correlate experimental viscosity data to temperature, an empirical correlation was used. Seeton (2006) reviewed existing viscosity-temperature relations and proposed an empirical correlation covering a wider range of temperatures than previous correlations. The Seeton (2006) correlation is utilized by several current oil-refrigerant studies, such as the Tangri *et al.* (2023) solubility study. This correlation is used to back out the mass fraction of refrigerant solved within oil. A similar design study was set up in this experiment, measuring viscosity, density, temperature, and pressure and utilizing thermodynamic correlations to determine the solubility of refrigerant and oil mixtures.

Most of these studies utilized a wide range of isolated experimentation to characterize either foaming, surface tension, or solubility. The required effort for collecting data is time consuming and exhaustive. Since Goswami *et al.* (1997), no comparable comprehensive foaming study which includes foam qualification, surface tension, and solubility studies has been performed on a wide range of relevant oil-refrigerant mixtures. This work is purposed with becoming an all-in-one experimental apparatus that rapidly collects similar data for oil-refrigerant mixtures and foams, maintaining the fidelity of isolated experiments, and performing a large, comprehensive foaming study for several low-GWP refrigerant and oil pairs.

2. EXPERIMENTAL APPARATUS DESIGN

2.1 Overview

A P&ID diagram of the developed apparatus can be seen in Figure 1, detailing the highlighted loops for study, positioning of sensors, and devices. The apparatus is centered by a “Main Chamber” which contains the primary sample of oil and refrigerant to be tested. Along the main chamber are various connections that run to the custom-design sight glass (“SG”) and the three experimental loops: Loop 1, which tests foam growth and decay, Loop 2, which tests interfacial dynamic surface tension, and Loop 3, which tests the solubility of refrigerant dissolved within oil. Each of these loops are highlighted in a unique color in Figure 1, and the key provides information regarding the symbols used in the P&ID.

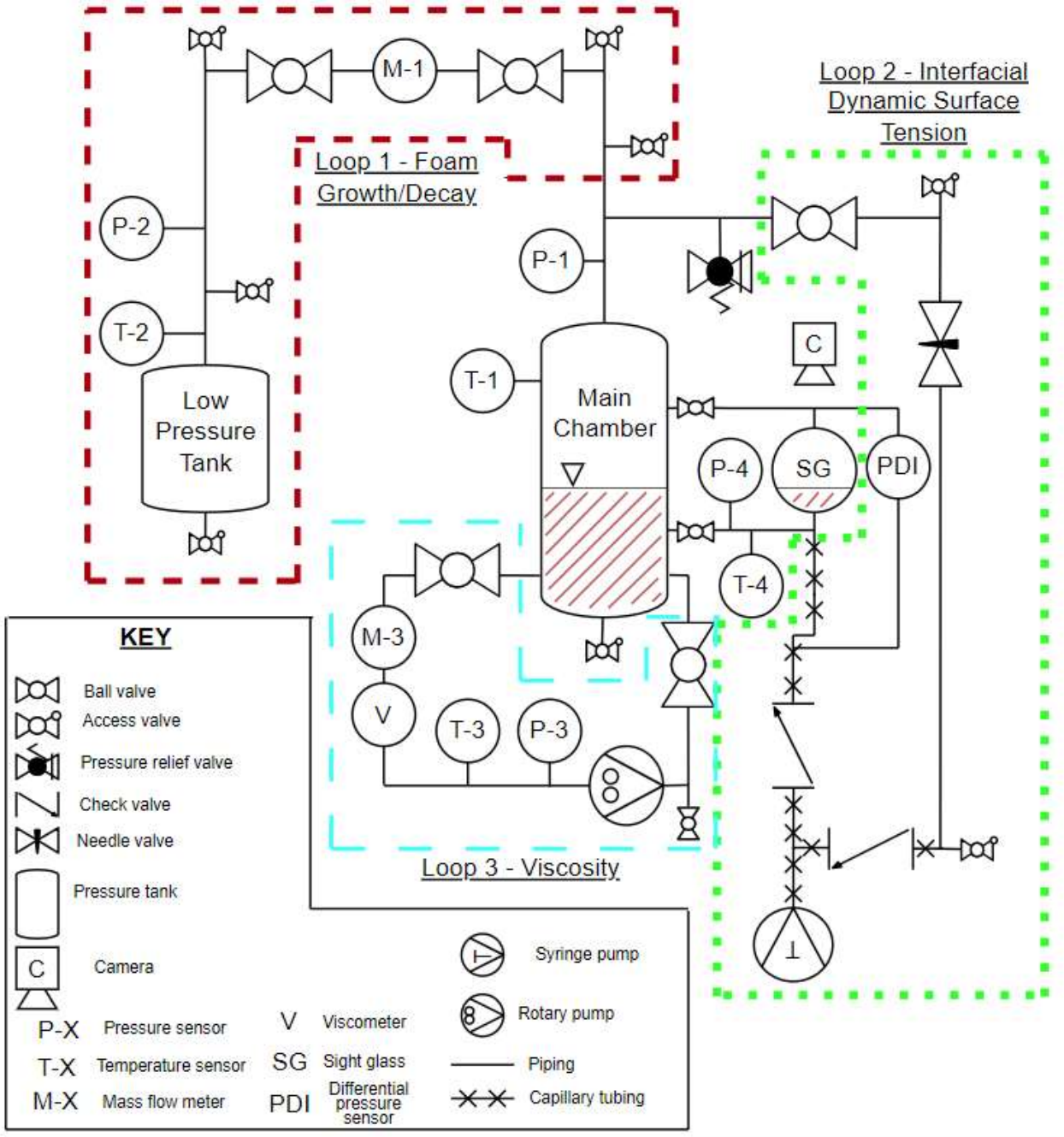

Figure 1 P&ID diagram for the Foamability Project experimental apparatus.

2.2 Main Chamber and Sight Glass

The main chamber is an ASME pressure-rated vessel of which refrigerant and oil are charged and is connected to a custom sight glass. As part of the goal of this project is to simulate the conditions within a compressor, the main chamber is sized approximately to that of a common scroll compressor. The internal volume is devoid of any components that might be seen inside of a compressor. The thermodynamic conditions in the vessel volume of the main chamber are measured directly via resistance temperature detectors (RTDs) and pressure transducers in the main chamber (T-1, P-1, for free vapor refrigerant, T-4 and P-4 for the mixture). T-1 and P-1 are exposed directly to the refrigerant vapor, and T-4 and P-4 are submerged in the oil-refrigerant mixture in the base of the sight glass.

Of the existing foaming experiments, most use similarly sized clear vessels to visualize foaming. For pressure drop-induced foaming, Goswami *et al.* 1998 and Barbosa *et al.* 2015 utilized similarly dimensioned cylindrical glass vessels. The advantage of a cylindrical shape is that it provides full visualization. As this experiment seeks to best emulate real compressor conditions, refrigerant is charged to saturation pressure for a given temperature. It is expected that the highest saturation temperature will be roughly 55°C, which corresponds to approximately 3400 kPa for R32, the highest pressure refrigerant to be tested. Most conventional cylindrical sight glasses cannot withstand such high pressures. Therefore, a concentric, double-tube, sight glass has been designed with a pressurized external annulus of water, shown in Figure 2.

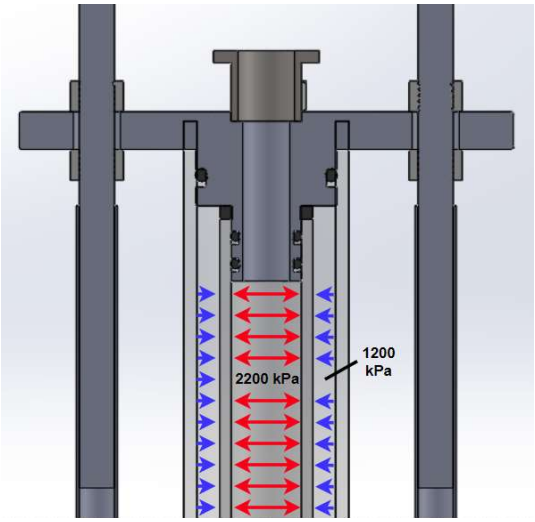

Figure 2 Pressure diagram cutout for the designed sight glass.

The custom sight glass contains a layer of pressurized water surrounding a borosilicate glass tube. This water is held within a plastic tube. The pressurized water reduces the effective pressure upon the glass tube and increases the potential testing pressures of oil and refrigerants to desired pressures. The selected glass tubes are 300 mm (12 in) long and have an approximate 18.4mm (0.725 in) ID and are rated up to 2200 kPa (325 psi). At a water pressure of 1200 kPa, an effective experimental pressure of 3400 kPa can be achieved.

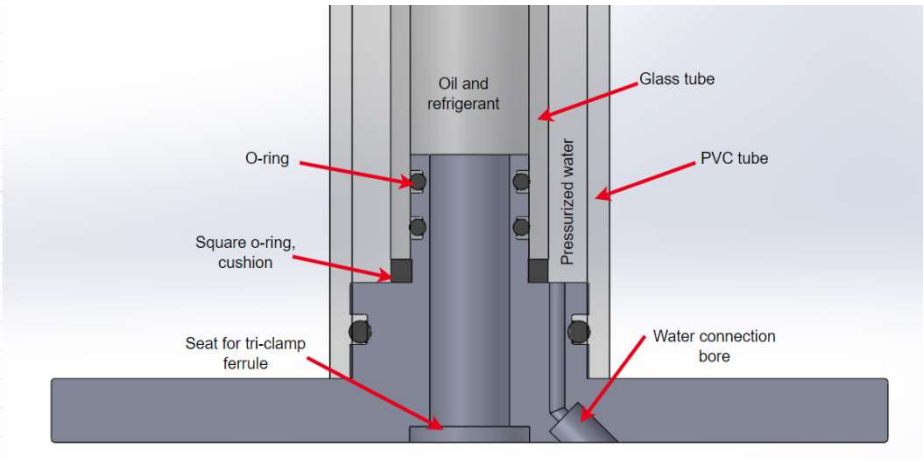

Figure 3 Cutout of the internal design of the sight glass flange and assembly.

Figure 3 highlights the internal volumes of the glass and plastic tubes that are separated and radially sealed with o-rings, designed to the Parker-Hannifin O-Ring Handbook (Parker Hannifin Corporation (2021)). Many elastomers are not compatible with refrigerants and oils, so a brief survey of existing compatibility literature was performed. Using Majurin *et al.* (2014), considering compressibility requirements for proper gas sealing, and availability of materials, EPDM o-rings were chosen for o-ring material. At the base of the glass tube lies a square o-ring cushion. Bored in the

flange is a water connection line to connect to a hydrostatic hand pump, which allows the water to be manually pressurized. Similarly, a seat is bored into the center bottom of the flange to braze a tri-clamp ferrule into the base of the flange, making assembly and disassembly of the sight glass uncomplicated. The two sight glass flanges are assembled together with threaded rods and secured with nuts and lock washers. The final assembly together is pictured in Figure 4. This final design is assembled and hydrostatically tested with water and later with nitrogen to ensure proper sealing and pressure tolerances.

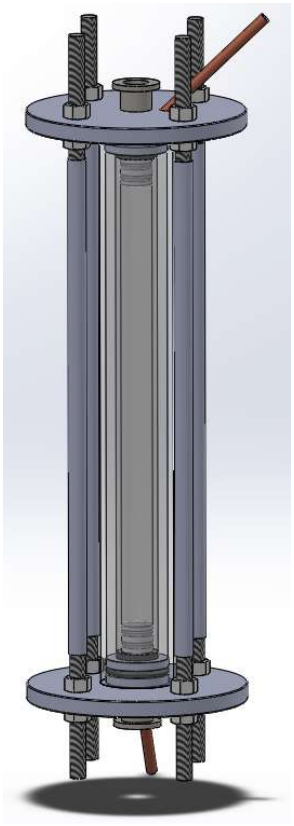

Figure 4 Complete rendering of the final sight glass assembly.

2.3 Loop 1 – Foamability

Loop 1, highlighted in Figure 1 above and to the left of the main chamber, is purposed with generating foam via pressure drop and studying its growth and decay. An oil-refrigerant mixture is charged to saturation pressure in the main chamber and heated to a desired temperature. This main chamber tank is separated from a low-pressure tank by two closed valves. The low-pressure tank is evacuated and brought to vacuum, depending on desired pressure differential between the tanks. When the system is at desired conditions and the tanks at respective equilibrium, the valves are opened between the tanks. This causes free refrigerant to evacuate from the main chamber to the low-pressure tank due to pressure difference. Refrigerant solved within the oil and present as a liquid beneath the oil evacuates the due to concentration and pressure gradients, causing bubble and foam generation. As the tanks reach equilibrium, the foam column drains and decays.

The low-pressure tank was initially sized to an approximately similar but larger volume to that of the main chamber to instigate a large enough volume for the refrigerant vapor to expand into and create a sufficient pressure drop. The low-pressure tank temperature and pressure are measured directly with the same instrumentation (T-2, P-2) as the main chamber. Refrigerant mass flow and density is measured with a Coriolis mass flow meter (M-1). The foam column is visualized with a custom sight glass (see SG in Figure 1, detailed in Section 2.2). Foam growth and decay are measured via a high-speed camera and post-processing software which tracks the foam column frame-by-frame with OpenCV, an open-source camera-tracking package in Python.

2.4 Loop 2 – Interfacial Dynamic Surface Tension

Loop 2, highlighted in Figure 1 to the right of the main chamber, is purposed with generating refrigerant bubbles within the oil-refrigerant mixture and measuring the interfacial surface tension via maximum bubble pressure tensiometry (MBPT). Following the top of the main chamber, refrigerant is drawn through a check valve into a syringe pump seen at the bottom and discharged through another check valve into a needle in the sight glass. The syringe pump allows for precise control of the refrigerant flowrate and utilizes a special gas-tight syringe. The gaseous refrigerant is discharged into a capillary needle turned downward into the oil-refrigerant liquid mixture bulk, seen in Figure 5.

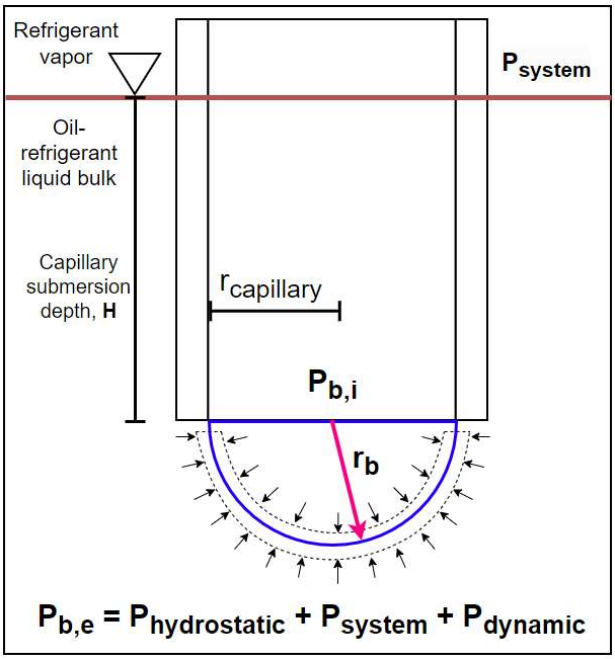

Figure 5 Pressure diagram for the maximum bubble pressure tensiometry method test.

The maximum bubble pressure tensiometry (MBPT) method relies upon the observation that the maximum pressure within a growing bubble is achieved when the radius of the bubble (r_b) is equal to the capillary radius ($r_{capillary}$). So, when measuring the internal bubble pressure, one can determine the approximate radius of the bubble when the internal bubble pressure reaches a maximum. The Young-Laplace equation is used to determine the surface tension of the interface between two fluids,

$$\Delta P = \gamma \nabla \cdot \hat{n} = \gamma \left(\frac{1}{R_1} + \frac{1}{R_2}\right) = \frac{2\gamma}{r_b}. \tag{1}$$

Pressure difference across the bubble surface is comprised of internal bubble pressure ($P_{b,i}$) and external bubble pressure ($P_{b,e}$). External bubble pressure ($P_{b,e}$) consists of systematic pressure (P_{system}) and hydrostatic pressure (P_H), however at high gas flowrates the bubble will experience resistive pressure in the form of aerodynamic, viscous, and inertial effects (Liggieri, Mileva, Miller (2019)), which is referred to as resistive pressure. This resistive pressure (P_R) is considered negligible for low flowrate conditions as such forces are all functions of velocity and acceleration. Summing up these forces, we have a total equation for pressure difference across the bubble, and can implement it in (equation 2) and solve for surface tension,

$$\gamma = \frac{r_b(P_{b,i} - P_{system} - \rho g\ )}{2}. \tag{2}$$

Further dimensions of bubbles can be measured via a high-speed camera and OpenCV image-tracking. The pressure difference between the bubble and surrounding vapor often measures to just a few Pascals and is measured with a differential pressure sensor (PDI). Hydrostatic pressure can be estimated in post-processing with camera-tracking height data and thermodynamic conditions.

2.5 Loop 3 – Solubility

Loop 3, highlighted in Figure 1 below the main chamber, is purposed for measuring the solubility of refrigerant within oil. It uses an oscillating-piston viscometer (V) paired with density data from a Coriolis mass flow meter (M-3). An RTD and a pressure sensor (T-3, P-3) measure the oil-refrigerant mixture temperature and pressure. An oil pump is controlled with a voltage output module and a drive and moves the oil-refrigerant mixture through the Loop 3 piping and instrumentation. Determining solubility, or the mass fraction of refrigerant solved within the oil, is done by directly measuring thermodynamic data such as viscosity, density, temperature, and pressure, and solving a thermodynamic model with the generated data.

To test for solubility, a known mass of oil and refrigerant is added to the system. Some portion of this refrigerant dissolves within the oil. After reaching thermodynamic equilibrium, the mixture is pumped across the instrumentation and data is collected. Due to oil sample variability, samples are provided to and oil data is collected by ASHRAE RP1879 sponsors. Pure refrigerant data is derived from EES. Combining pure oil and refrigerant data with measured data, a thermodynamic model can be used to determine solubility. Combined with density data from the Coriolis mass flow meter, the viscometer data records both dynamic and kinematic viscosity. With temperature and solubility data, Daniel plots, as in Figure 6 from Barthel and Majurin (2019), can be generated for the oil-refrigerant mixture showing the variance in viscosity relative to temperature and solubility.

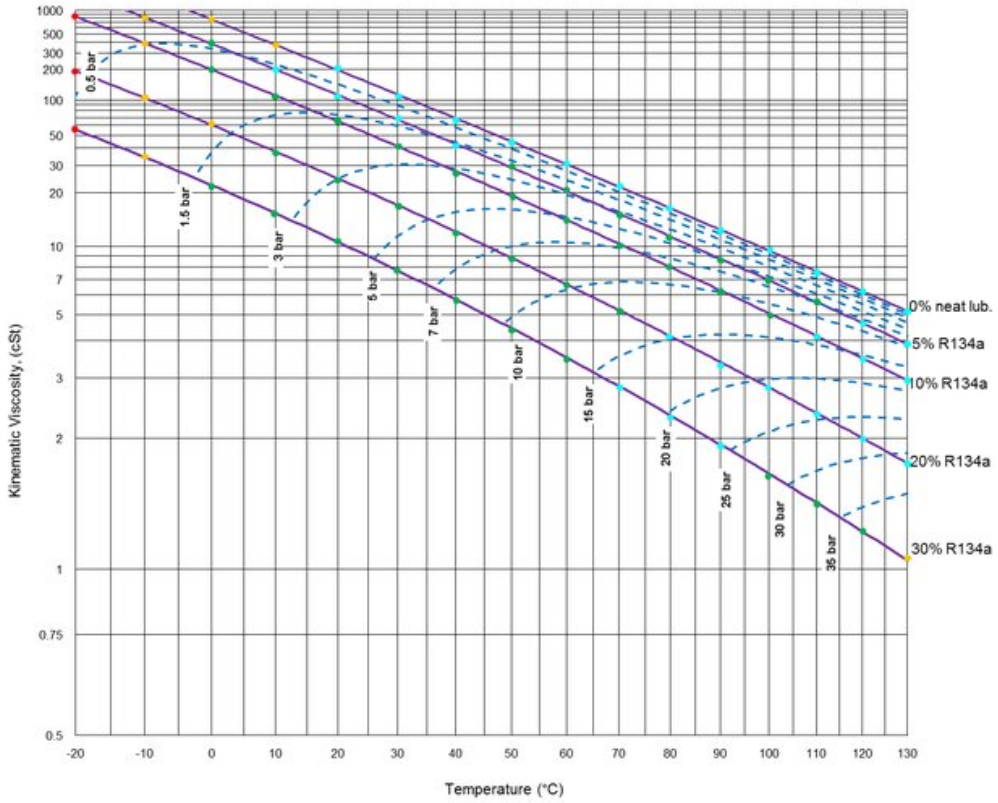

Figure 6 A Daniel plot sourced from Barthel and Majurin (2019).

2.6 Devices and Instrumentation

Below in Table 1 lies a listing of instruments and components utilized in the apparatus, including types, models, performance ranges, and systematic accuracy.

Table 1 Device and instrument specifications.

Device Type	Model Number	Performance Range	Accuracy
Pressure Transducer (P-X)	Danfoss 060G1146	0 - 750 psi	± 1% FS
Platinum RTD (T-X)	Danfoss 084N2031	-60 - 180°C	± 0.7°C

Differential Pressure Transducer (PDI)	Validyne CD16-A-1-D	0 - 0.125 psi	± 0.5% FS
Coriolis Mass Flow Meter (M-1)	Micro Motion CMF050M322MB	0 – 6800 kg/hr	± 0.1% for mass flow ± 0.5 kg/m3 for density
Coriolis Mass Flow Meter (M-3)	Micro Motion CMF025M321NABMEZZZ	0 – 2180 kg/hr	± 0.1% for mass flow ± 0.5 kg/m3 for density
Vibrating-Piston Viscometer	Hydramotion XL7-900-T15-20K	0 – 1100 cP	± 1.14 cP
DAQ Chassis	National Instruments cDAQ-9174	N/A	N/A
DAQ Current Input Module	National Instruments NI-9203	± 20 mA, 16 bits	N/A
DAQ Voltage Output Module	National Instruments NI-9263	± 10 VDC, 16 bits	N/A
DAQ Voltage Input Module	National Instruments NI-9226	0-4000 Ω, 24 bits	± 0.5°C

All instruments are connected to various modules within a National Instruments CompactDAQ chassis and controlled and processed with a LabView module. The syringe pump utilized is a Kent Scientific GenieTouch™ syringe pump, with variable flowrates ranging 0.0001 µL/hr – 220.82 mL/min. The oil pump used is a Micropump GC-M25.PVS.E Gear Pump. The final apparatus also contains a safety circuit connected to an emergency stop and high-pressure switch. For further pressure safety, an adjustable spring safety valve connected in line with a diaphragm safety valve and a refrigerant recycling tank.

3. UNCERTAINTY AND TEST PROCEDURES

3.1 Uncertainty

Pressure transducers and RTDs were calibrated in lab and verified by comparing pressure and temperature data for refrigerants in EES. Mass flow meter performance was verified with water and nitrogen tests. The differential pressure transducer was calibrated by the manufacturer and can be recalibrated with a differential pressure manometer. The viscometer was calibrated by the manufacturer with standardized oils. Final uncertainty propagation is analyzed via ASME PTC 19.1-2013 for total uncertainty $u_{\bar{X}}$ (equation 3), systematic uncertainty $s_{\bar{x}}$ (equation 4), and random uncertainty $b_{\bar{X}}$,

$$u_{\bar{X}} = \sqrt{(b_{\bar{X}})^2 + (s_{\bar{x}})^2} \tag{3}$$

$$s_{\bar{x}} = \frac{1}{\sqrt{N}}\sqrt{\frac{\sum_{j=1}^{N}(X_j - \bar{X})^2}{N-1}} \qquad b_{\bar{X}} = \sqrt{\frac{1}{N_{\beta_{\bar{X}_k}}}\sum_{j=1}^{N_{X_k}}\frac{\left(X_{k_j} - \bar{X}_k\right)^2}{N_{X_k}-1}}. \tag{4) (5}$$

Final uncertainty propagation will be analyzed in post-processing.

3.2 Test Procedures

The entire apparatus is flushed with acetone and purged with nitrogen until negligible amounts of distillate remain to ensure fluid purity and avoid contamination. To begin testing, the system is pulled to vacuum. A mass of oil is inserted into the system measured with a scale and then the system is again pulled to vacuum to remove entrapped vapors and moisture within the oil. A temperature-controlled enclosure is set to a desired temperature. Refrigerant is charged into the system until saturation pressure for the desired temperature is achieved. To ensure saturation, the pressure measured in the system is compared with saturation pressure data in EES. Refrigerant mass inserted into the system is recorded with a scale. Then, the oil pump is turned on to encourage solving of the refrigerant into the oil, and the system is let to rest. Once equilibrium is met, testing begins with the three different experimental loops.

4. CONCLUSIONS AND FUTURE WORK

An all-in-one apparatus capable of qualifying and quantifying oil-refrigerant mixture foams has been developed to study foam growth and decay, interfacial dynamic surface tension, and solubility. The apparatus is designed to rapidly and reliably perform these experiments for a variety of oil and refrigerant pairs from 20°C to 55°C up to a pressure of 3400 kPa. This range of conditions and testing pairs exceeds previous studies and is planned to provide a wide set of data purposed for designing HVAC&R systems with low-GWP refrigerant and oil pairs.

Currently, the Foamability Project experimental apparatus is being refined and tested with preliminary pairings R134a and 32 ISO POE, R22 and 68 ISO mineral oil. As an experimental control, additive-free POE oil is tested alongside off-the-shelf POE oil. These preliminary test pairs will be compared with foam and surface tension data from Goswami *et al*. 1998 and solubility data from ASHRAE RP1879 sponsors. Once testing is refined and verified with comparative data, experimentation upon the previous matrix of pairings in Table 2 will be performed at saturation pressures from approximately 20°C to 55°C.

Table 2 Refrigerant and oil testing matrix for project.

Ref. (right)/ Oil (below)	R1234zeE	R1234yf	R1233zd	R454B	R32
POE	X	X	X	X	X
PVE		X		X	X
PAG	X				X
MO			X		

NOMENCLATURE

Symbol	Description	Units
ΔP	Differential pressure	Pa
γ	Surface tension	N/m
r_b	Bubble radius	m
$r_{capillary}$	Capillary radius	m
$P_{b,i}$	Internal bubble pressure	Pa
$P_{b,e}$	External bubble pressure	Pa
P_{system}	Systematic pressure	Pa
ρ	Density	kg/m^3
g	Gravity constant	kg/m-s^2
H	Capillary depth	m
$u_{\bar{X}}$	Total uncertainty	---
$s_{\bar{x}}$	Systematic uncertainty	---
$b_{\bar{X}}$	Random uncertainty	---

REFERENCES

American Society for Testing and Materials (ASTM). (2018). ASTM D892-Standard Test Method for Foaming Characteristics of Lubricating Oil. West Conshohocken, PA.

American Society for Testing and Materials (ASTM). (n.d.). ASTM D892-Standard Test Method for Foaming Characteristics of Lubricating Oil. West Conshohocken, PA.

American Society of Mechanical Engineering (ASME). (2013). PTC-19.1-2013 Test Uncertainty. New York, NY.

Barthel, A. J., & Majurin, J. (2019). Understanding and improving the 9-coefficient pressure viscosity temperature (PVT) model. *International Conference on Compressors and their Systems*.

Fainerman, V., & Miller, R. (2004). Maximum bubble pressure tensiometry - an analysis of experimental constraints. *Advances in Colloid and Interface Science*, 287-301.

Fortkamp, F. P., & Barbosa Jr., J. R. (2015). Refrigerant desorption and foaming in mixtures of HFC-134a and HFO-1234yf and a polyol ester lubricating oil. *Internal Journal of Refrigeration*, 69-79.

Fukuta, M., Sumiyama, J., Motozawa, M., & Yanagisawa, T. (2017). Surface tension measurement of oil/refrigerant mixture by maximum bubble pressure method. *international Journal of Refrigeration*, 125-133.

Goswami, Y. D., Shah, D. O., Jotshi, C. K., Bhagwat, S. S., Leung, M., & Gregory, A. S. (1997). Foaming characteristics of HFC refrigerants. *ASHRAE Journal, 39*, 39-44.

Hung, J.-T., Chen, Y.-K., Chen, T.-Y., Sheng, S.-R., & Wang, C.-C. (2016). On the Effect of Lubricant on Pool Boiling Heat Transfer Performance. *International Refrigeration and Air Conditioning Conference*.

Lee, G., Fukuta, M., Motozawa, M., Kimura, R., & Tsujita, R. (2022). Surface Tension, Oil Level and Density Measurement of Oil/Refrigerant Mixture by Maximum Bubble Pressure Method. *International Refrigeration and Air Conditioning Conference*.

Liggieri, L., Mileva, E., & Miller, R. (2019). The Surface Layer as the Basis for Foam Formation and Stability. In *Foam Films and Foams Fundamentals and Applications* (pp. 3-53). Boca Raton, London, New York: CRC Press Taylor & Francis Group, Progress in Colloid and Interface Science.

Majurin, J. A., Gilles, W., & Staats, S. J. (2014). Materials Compatibility of HVACR System Materials with Low GWP Refrigerants. *International Refrigeration and Air Conditioning Conference*.

Parker Hannifin Corporation. (2021). *Parker O-Ring Handbook.* Cleveland, OH: Parker Hannifin Corporation.

Seeton, C. J. (2006). Viscosity-temperature correlation for liquids. *Tribology Letters, Vol. 22, No.1*, 67-78.

Seeton, C. J., & Hrnjak, P. (2009). Interfacial Tension of Mixtures of CO2 with POE and PVE Lubricants. *3rd IIR Conference on Thermophysical Properties and Transport Processes of Refrigerants.* Boulder, CO.

Tangri, H., Purohit, N., Sethi, A., & Hulse, R. (2023). Solubility, miscibility and compatibility studies of low GWP non-flammable refrigerants and lubricants for refrigeration and air conditioning applications. *International Journal of Refrigeration*, 45-63.

Wang, C.-C., Lin, Y. T., Chung, H. D., & Hu, Y. R. (1999). Some observations of foaming characteristics in the nucleate boiling performance of refrigerant-oil mixtures. *ASHRAE Transactions, 105*, 469.

Yanagisawa, T., Shimizu, T., & Fukuta, M. (1991). Foaming characteristics of an oil-refrigerant mixture. *International Journal of Refrigeration*.

Yokozeki, A. (1994). Solubility and Viscosity of Refrigerant-Oil Mixtures. *International Compressor Engineering Conference*.

ACKNOWLEDGEMENT

This project is supported by ASHRAE, project RP-1879. The authors are appreciative of the members of the Project Management Subcommittee that support this project including: Chris Seeton, Brad Boggess, Henna Tangri, Julie Majurin, Raymond Drost, Casey Scruggs, Valerie Lisi, Joe Karnaz, Sara Kampfe, and Sheli Porter.